GSA Data Repository 2015238

PART 1: THE DATA BASE

The following table summarizes the Mean Annual Temperature data used in this study. The paleolatitudes and paleolongitudes were initially generated using the Paleogeographic Information Systems (PGIS) program of Malcolm Ross and Christopher Scotese, and subsequently modified using the most recent version of Point Tracker by Christopher Scotese. The paleogeography used in the modeling study was generated with PGIS, and constitutes a modified version of that used by Upchurch et al. (Upchurch et al., 1999). We did our initial point rotations in PGIS to be compatible with model paleogeography, and modified them with updated data.

The data, calibrations, and sources of error are explained in the paragraphs following the table. Temperatures based on leaf margin analysis are explained more fully in Part 2.

Record No.	**Locality**	**Data type**	**Mean Annual Temperature °C**	**"Random" Error, °C (sampling, non-dissolution, error)**	**Error type**	**Modern latitude**	**Modern longitude**	**Paleo-Lati-tude**	**Paleo-Longi-tude**	**Source**
1	Alpha Ridge (uppermost Campanian to lower Maastrichtian)	$TEXH_{86}^{H}$	**17**	±2.5°	1 S.D., modern calibration error for $TEXH_{86}^{H}$(Kim et al., 2010)	85	-98	78	14	Recalculated from (Jenkyns et al., 2004)
2	Colville (upper Campanian)	Dinosaur $\delta^{18}0$	**3**	+3.1/-3°	Calculated from 95% C.I. shown in paper	70	-151	81	-132	Calculated from data in (Amiot et al., 2004)
3	Prince Creek Formation, North Slope (lower Maastrichtian)	Macroflora, Life Form Analysis	**5** (midpoint of range)	2–8°	MAT interval for extant equivalent vegetation	70	-151	81	-132	(Parrish and Spicer, 1988)
4	Prince Creek Formation,	Extrapolation of CLAMP	**6**	±2.8°	1 S.D., maximum error for CLAMP,	70	-151	81	-132	(Spicer and Herman, 2010)

	North Slope (Maastrichtian)	latitudinal gradient for Maastrichtian			extant data set					
5a	Cantwell Formation, Sable Mountain (lower Maastrichtian)	Macroflora, CLAMP	**7**	±2.8°	1 S.D., maximum error for CLAMP, extant data set	63.5	-149.8	74	-132	(Tomisch et al., 2010)
5b	Cantwell Formation, Sable Mountain (lower Maastrichtian)	Macroflora, Leaf margin analysis	**<8**	>±2.6°	1 S.D., sampling error for fossil assemblage	63.5	-149.8	74	-132	Calculated from data in (Tomisch, McCarthy et al. 2010)
6	Raryktin, NE Russia (Maastrichtian)	Macroflora, CLAMP	**11**	±2.8°	1 S.D., maximum error for CLAMP, extant data set	63	177	75	179	(Goloneva, 2000)
7	Kakanut, NE Russia (Maastrichtian)	Macroflora, CLAMP	**10**	±2.8°	1 S.D., maximum error for CLAMP, extant data set	63	174	75	174	(Goloneva, 2000)
8	Koryak, NE Russia (Maastrichtian)	Macroflora, CLAMP	**4**	±2.8°	1 S.D., maximum error for CLAMP, extant data set	60	168	70	168	(Moiseeva, 2005)
9	Koryak Upland (Maastrichtian)	Mollusc $\delta^{18}0$ (aragonite)	**10–17 (12)** n=4	±1.6°	1 S.E. for mollusk calibration data, (Grossman and Ku, 1986)	60	168	70	168	(Zakharov et al., 2006)
10	Chignik flora, Alaska (upper Campanian)	Macroflora, Leaf margin analysis	**13**	±3.2°	1 S.D., sampling error for fossils	56.3	-158.5	69	-147	This report
11	Lower Atanikerdluk flora, Greenland (Maastrichtian)	Macroflora, Leaf margin analysis	**24**	±2°	1 S.E. for Northern Hemisphere calibration data of (Wilf, 1997)	70	-52	61	-19	This report
12	Edmonton, Alberta (Maastrichtian)	Macroflora, CLAMP	**12**	±2.8°	1 S.D., maximum error for CLAMP, extant data set	53	-113.5	60	-88	(Goloneva, 2000)

13	Vilui, Siberia	Macroflora, CLAMP, modified for Maastrichtian (see part 3)	**11**	±2.8°	1 S.D., maximum error for CLAMP, extant data set	63.9	121.9	65	103	(Spicer et al., 2008; Spicer and Herman, 2010)
14a	Alberta (upper Campanian)	Crocodile $\delta^{18}0$	**12**	+1/-2.4°	Calculated from 95% C.I. shown in paper	50	-105	56	-80	Calculated from data in (Amiot et al., 2004)
14b	Alberta (upper Campanian)	Crocodile Modern Thermal Tolerances	**>14**	NA	Interval, MAT >14°	50	-105	56	-80	(Amiot et al., 2004; Markwick, 1998)
15	Alberta (upper Campanian)	Dinosaur $\delta^{18}0$	**10**	+2/-3.7°	Calculated from 95% C.I. shown in paper	50	-105	56	-80	Calculated from data in (Amiot et al., 2004)
16	Sakhalin, Russia (Maastrichtian)	Macroflora, CLAMP	**14**	±2.8°	1 S.D., maximum error for CLAMP extant data set	49	143	53	136	(Goloneva, 2000)
17	Sakhalin, Russia, Krasnoyarka Formation (Maastrichtian average)	Mollusc $\delta^{18}0$ (aragonite)	**7–11 (9)** n=10	±1.6°	1 S.E. of modern calibration data for mollusks in (Grossman and Ku, 1986)	47.3	142.5	51	136	(Zakharov et al., 2006)
18	Montana (upper Campanian)	Crocodile $\delta^{18}0$	**14**	+1.1/-1°	Calculated from 95% C.I. shown in paper	46	-105	52	-82	Calculated from data in (Amiot et al., 2004)
19	Montana (upper Campanian)	Dinosaur $\delta^{18}0$	**10**	+2.8/-1.3°	Calculated from 95% C.I. shown in paper	46	-105	52	-82	Calculated from data in (Amiot et al., 2004)
20a	Hell Creek, North Dakota (upper Maastrichtian)	Macroflora, CLAMP	**12**	±2.8°	1 S.D., maximum error for CLAMP, extant data set	46.3	-103.9	52	-80	(Goloneva, 2000)
20a	Hell Creek, North Dakota (upper Maastrichtian)	Macroflora, Leaf margin analysis, lowest value	**7**	±2°	1 S.E. for Northern Hemisphere calibration data	46.3	-103.9	52	-80	(Wilf et al., 2003)

					of (Wilf, 1997)					
20a	Hell Creek, North Dakota (upper Maastrichtian)	Macroflora, Leaf margin analysis, highest value	**18**	±2.5°	1 S.D. sampling error for fossil assemblage	46.3	-103.9	52	-80	(Wilf et al., 2003)
20b	Fox Hills, North Dakota (upper, not uppermost Maastrichtian)	Digital Leaf Physiognomy North American model	**17**	3.3°	1 S.D. of calibration data, North American regression model	46.3	-103.9	52	-80	(Peppe et al., 2011)
21	Fox Hills, South Dakota (upper, not uppermost Maastrichtian)	Mollusc $\delta^{18}0$ (aragonite)	**18–21 (19)** n=4	±1.6°	1 S.E. of modern calibration data for mollusks in (Grossman and Ku, 1986)	45.5	-100.7	50	-78	(Zakharov et al., 2006)
22	Fox Hills, South Dakota (upper, but not uppermost, Maastrichtian)	Fish otolith $\delta^{18}0$ (carbonate)	**18**	±1.6°	1 S.E. of modern calibration data for mollusks in (Grossman and Ku, 1986)	45	-100.7	50	-78	(Carpenter et al., 2003)
23a	Medicine Bow (upper Maastrichtian)	Macroflora, CLAMP	**16–17**	±2.8°	1 S.D., maximum error for CLAMP, extant data set	41.9	-107	48	-86	(Goloneva, 2000; Wolfe, 1990)
23b	Medicine Bow (upper Maastrichtian)	Macroflora, Leaf margin analysis	**20**	±2.4°	1 S.D., sampling error for fossil assemblage	41.9	-107	48	-85	This report
24a	Lance (upper Maastrichtian)	Macroflora, CLAMP	**14–16**	±2.8°	1 S.D., maximum error for CLAMP, extant data set	43.1	-104.6	49	-84	(Goloneva, 2000; Wolfe, 1990)
24b	Lance (upper Maastrichtian)	Macroflora, Leaf margin analysis	**20**	±2.4°	1 S.D. sampling error for fossil assemblage	43.1	-104.6	49	-84	This report
25a	Maastricht, Netherlands (Maastrichtian)	Fish tooth enamel $\delta^{18}0$	**14**	±1.2°	1 S.E. for modern calibration data, equation 2 of (Lécuyer et al.,	50.9	5.7	44	4	(Puceat et al., 2007), (Lécuyer et al., 2013) recalibration

					2013)					
25b	Maastricht, Netherlands (Maastrichtian)	Fish tooth enamel $\delta^{18}0$	**18**	±2.7°	1 S.E. for modern calibration data, equation 2 of (Pucéat et al., 2010)	50.9	5.7	44	4	(Puceat et al., 2007), (Pucéat et al., 2010) recalibration
26a	Nasilov, Poland (Maastrichtian-Danian boundary)	Fish tooth enamel $\delta^{18}0$	**15–20 (17)** n=3	±1.2°	1 S.E. for modern calibration data, equation 2 of (Lécuyer et al., 2013)	51.3	22	44	19	(Puceat et al., 2007), (Lécuyer et al., 2013) recalibration
26b	Nasilov, Poland (Maastrichtian-Danian boundary)	Fish tooth enamel $\delta^{18}0$	**19–23 (20)** n=3	±2.7°	1 S.E. for modern calibration data, equation 2 of (Pucéat et al., 2010)	51.3	22	44	19	(Puceat et al., 2007), (Pucéat et al., 2010) recalibration
27	South Netherlands (uppermost Maastrichtian)	Mollusc $\delta^{18}0$	**20**	±1.6°	1 S.E. of modern calibration data for mollusks in (Grossman and Ku, 1986)	50.9	5.7	44	4	(Zakharov et al., 2006)
28a	Littleton (upper Maastrichtian)	Macroflora, CLAMP	**17**	±2.8°	1 S.D., maximum error for CLAMP extant data set	39.6	-105	46	-84	(Wolfe, 1990)
28b	Littleton (upper Maastrichtian)	Macroflora, Leaf margin analysis	**22**	±2°	1 S.E. for North American calibration data of (Wilf, 1997)	39.6	-105	46	-84	This report
29a	Laramie (upper Maastrichtian)	Macroflora, CLAMP	**19**	±2.8°	1 S.D., maximum error for CLAMP extant data set	39.6	-105	46	-84	(Wolfe, 1990)
29b	Laramie, lower floras (upper Maastrichtian)	Macroflora, Leaf margin analysis	**26**	±2°	1 S.E. for North American calibration data	39.6	-105	46	-84	This report

					of (Wilf, 1997)					
29b	Laramie, Broomfield (upper Maastrichtian)	Macroflora, Leaf margin analysis	**23**	±3.1°	1 S.D. sampling error for fossil assemblage	39.6	-105	46	-84	This report
30	Zaisan, Kazakhstan (Maastrichtian)	Macroflora, CLAMP	**11**	±2.8°	1 S.D., maximum error for CLAMP extant data set	48	84.9	45	67	(Goloneva, 2000)
31a	Vermejo (upper Maastrichtian)	Macroflora, CLAMP	**18**	±2.8°	1 S.D., maximum error for CLAMP extant data set	37	-104.5	43	-85	(Wolfe, 1990)
31b	Vermejo (upper Maastrichtian)	Macroflora, Leaf margin analysis	**23**	±2°	1 S.E. for North American calibration data of (Wilf, 1997)	37	-104.5	43	-85	This report
32a	Lower Raton (uppermost Maastrichtian)	Macroflora, CLAMP	**18**	±2.8°	1 S.D., maximum error for CLAMP extant data set	37	-104.5	43	-85	(Wolfe, 1990)
32b	Lower Raton (uppermost Maastrichtian)	Macroflora, Leaf margin analysis	**23**	±2.1°	1 S.D., sampling error for fossil assemblage	37	-104.5	43	-85	This report
33a	New Jersey (Maastrichtian average)	Fish tooth enamel $\delta^{18}0$, one or more sites	**14–29 (19)** n = 10	±1.2°	1 S.E. for modern calibration data, equation 2 of (Lécuyer et al., 2013)	40	-75	40	-52	(Puceat et al., 2007), (Lécuyer et al., 2013) recalibration
33b	New Jersey (Maastrichtian average)	Fish tooth enamel $\delta^{18}0$, one or more sites	**17–32 (22)** n = 10	±2.7°	1 S.E. for modern calibration data, equation 2 of (Pucéat et al., 2010)	40	-75	40	-52	(Puceat et al., 2007), (Pucéat et al., 2010) recalibration
34	McRae Formation, Jose Creek Member (upper Campanian or	Macroflora, Leaf margin analysis	**22**	±2.3°	1 S.D. sampling error for fossil assemblage	33.2	-107.2	40	-88	This report

	lower Maastrictian)									
35a	Ripley (lower Maastrichtian)	Macroflora, CLAMP	**17**	±2.8°	1 S.D., maximum error for CLAMP extant data set	35	-88.4	38	-68	(Goloneva, 2000; Wolfe, 1990)
35b	Ripley, Cooper (lower Maastrichtian)	Macroflora, Leaf margin analysis	**22**	±2.4°	1 S.D. sampling error for fossil assemblage	36	-88	38	-68	This report
35b	Ripley, Perry (lower Maastrichtian)	Macroflora, Leaf margin analysis	**23**	±2.1°	1 S.D. sampling error for fossil assemblage	36	-88	38	-68	This report
36	Tennessee (upper Campanian)	Mollusc $\delta^{18}0$	**18–22 (20)** n =4	±1.6°	1 S.E. of modern calibration data for mollusks in (Grossman and Ku, 1986)	35.4	-88.4	39	-68	(Zakharov et al., 2006)
37	France (upper Campanian to lower Maastrichtian)	Crocodile $\delta^{18}0$	**21**	±1°	Calculated from 95% C.I. shown in paper	43	3	36	1	Calculated from data in (Amiot et al., 2004)
38	France (upper Campanian to lower Maastrichtian)	Dinosaur $\delta^{18}0$	**23**	+2.1/-2°	Calculated from 95% C.I. shown in paper	43	3	36	1	Calculated from data in (Amiot et al., 2004)
39	Texas (upper Campanian to lower Maastrichtian)	Crocodile $\delta^{18}0$	**19**	±1.1°	Calculated from 95% C.I. shown in paper	30	-103	36	-85	Calculated from data in (Amiot et al., 2004)
40	Texas (upper Campanian to lower Maastrichtian)	Dinosaur $\delta^{18}0$	**20**	+1/-1.1°	Calculated from 95% C.I. shown in paper	30	-103	36	-85	Calculated from data in (Amiot et al., 2004)
41	Big Bend, Texas (Maastrichtian)	Soil carbonate $\delta^{18}0$	**15**	±0.5°	Analytic error only	30	-103	36	-85	(Dworkin et al., 2005)
41	Big Bend, Texas	Soil carbonate	**22**	±0.5°	Analytic error	30	-103	36	-85	(Dworkin et al.,

	(Maastrichtian)	$\delta^{18}0$			only					2005)
42	Baja CA, Rosario Fm., San Antonio del mar section[1] (upper Campanian to lower Maastrichtian)	High temp planktonic foraminifera $\delta^{18}0$, salinity corrected	**26–30**	±2.9°	1 S.D. core top error for Holocene planktonic foraminifera (Crowley and Zachos, 2000)	31	-116.2	36[1]	-96	(Maestas et al., 2003)
43a	Olmos (upper Campanian to lower Maastrichtian)	Macroflora, CLAMP	**24**	±2.8°	1 S.D., maximum error for CLAMP extant data set	27.5	-101	33	-83	Jack Wolfe, oral communication, 2005
43b	Olmos (upper Campanian to lower Maastrichtian)	Macroflora, Leaf margin analysis	**25**	±2°	1 S.E. for North American calibration data of (Wilf, 1997)	27.5	-101	33	-83	Recalculation of data compiled by (Estrada-Ruiz et al., 2008)
44	Shuqualak Core, Mississippi, USA (Maastrichtian average)	TEX_{86}^{H}	**27–31 (30)** n=9	±2.5°	1 S.D., modern calibration for $TEXH_{86}^{H}$, (Kim et al., 2010)	33	-88.5	36	-67	TEX_{86}^{H} temperatures calculated from supplementary data of (Linnert et al., 2014)
45	Corsicana Fm., Brazos River Cretaceous-Tertiary boundary section (upper Maastrichtian)	TEX_{86}^{H}	**30** n= 7	±2.5°	1 S.D., modern calibration for $TEXH_{86}^{H}$ (Kim et al., 2010)	31	-97	36	-77	TEX_{86}^{H} temperatures provided by (Vellekoop et al., 2014)
46	Mullinax-1 and Mullinax-3 cores, Falls County, Texas (upper Maastrichtian)	Very well preserved (non-recrystallized) foraminifera encased in	**27 (28 max)** (Maximum T, inferred SST, average for *Pseudoguem belina*	±2.9°	1 S.D. core top error for Holocene planktonic foraminifera (Crowley and	31	-97	36	-77	Calculated from (Ashckenazi-Polivoda et al., 2014) using equation of (Hays and Grossman,

		clay, $\delta^{18}0$	*costulata,* max. from Table 3)		Zachos, 2000)					1991)
47a	Morocco (Maastrichtian average)	Fish tooth enamel $\delta^{18}0$, one or more sites	**24–31 (28)** n=15	±1.2°	1 S.E. for modern calibration data, equation 2 of (Lécuyer et al., 2013)	31.7	-8	23	-10	(Puceat et al., 2007), (Lécuyer et al., 2013) recalibration
47b	Morocco (Maastrichtian average)	Fish tooth enamel $\delta^{18}0$, one or more sites	**27–34 (31)** n=15	±2.7°	1 S.E. for modern calibration data, equation 2 of (Pucéat et al., 2010)	31.7	-8	23	-10	(Puceat et al., 2007), (Pucéat et al., 2010) recalibration
48a	Tunisia (lower Maastrichtian)	Fish tooth enamel $\delta^{18}0$	**24–30 (27)** n= 2	±1.2°	1 S.E. for modern calibration data, equation 2 of (Lécuyer et al., 2013)	36	9	25	7	(Ounis et al., 2008), (Lécuyer et al., 2013) recalibration
48b	Tunisia (lower Maastrichtian)	Fish tooth enamel $\delta^{18}0$	**28–33 (30)** n= 2	±2.7°	1 S.E. for modern calibration data, equation 2 of (Pucéat et al., 2010)	36	9	25	7	(Ounis et al., 2008), (Pucéat et al., 2010) recalibration
49a	Israel (Maastrichtian)	Fish tooth enamel $\delta^{18}0$, one or more sites	**19–22 (21)** n=3	±1.2°	1 S.E. for modern calibration data, equation 2 of (Lécuyer et al., 2013)	32	34.5	18	29	(Puceat et al., 2007), (Lécuyer et al., 2013) recalibration
49b	Israel (Maastrichtian)	Fish tooth enamel $\delta^{18}0$, one or more sites	**23–25 (24)** n=3	±2.7°	1 S.E. for modern calibration data, equation 2 of (Pucéat et al.,	32	34.5	18	29	(Puceat et al., 2007), (Pucéat et al., 2010) recalibration

					2010)					
50	Israel, Aderet 1 borehole (Maastrichtian average)	TEX_{86}^{H}	**26–30 (28)** n=23	±2.5	1 S.D., modern calibration for TEX_{86}^{H}, (Kim et al., 2010)	32	34.5	19	29	TEX_{86}^{H} temperatures calculated from data in (Alsenz et al., 2013)
51	Israel, PAMA Quarry (Efe syncline) (Maastrichtian average)	TEX_{86}^{H}	**24–29 (27)** n=18	±2.5	1 S.D., modern calibration for $TEXH_{86}^{H}$, (Kim et al., 2010)	32	34.5	19	29	TEX_{86}^{H} temperatures calculated from data in (Alsenz et al., 2013)
52	Jamaica (66.0 & 69.1 myr)	Rudist $\delta^{18}0$, midpoint of seasonal range	**32** n=2	±1.6°	?1 S.E. of modern calibration data for mollusks in (Grossman and Ku, 1986)	18.1	-78	18	-78	Calculated from supplementary data in (Steuber et al., 2005) using the equation of (Hays and Grossman, 1991)
53	Oman, Jebel Rawdah (69.1 myr)	Rudist $\delta^{18}0$, midpoint of seasonal range	**31–34 (32)** n=2	±1.6°	?1 S.E. of modern calibration data for mollusks in (Grossman and Ku, 1986)	24.7	54.8	6	46	Calculated from supplementary data in (Steuber et al., 2005) using the equation of (Hays and Grossman, 1991)
54	Wobejebato Guyot (69±1myr)	Rudist $\delta^{18}0$ (aragonite)	**30–32 (32)**	±1.2°	Precision for temperature in proposed modern analog *Arctica islandica* (Weidman et al., 1994)	12	164.9	0	-164	Calculated from (Wilson and Opdyke, 1996) using their equation and the equation of (Grossman and Ku, 1986)
55	Bolivia (middle Maastrichtian)	Crocodile $\delta^{18}0$	**25**	+3/-2.5°	Calculated from 95% C.I. shown in paper	-18	-65	-21	-51	Calcluated from data in (Amiot et al., 2004)
	Southern	Glassy	**31**	±2.9°	1 S.D. core top	-8	39	-21	30	(Pearson et al.,

	coastal Tanzania (67±2 myr)	foraminifera encased in clay, $\delta^{18}0$	(Warmest T, inferred SST)		error for Holocene planktonic foraminifera (Crowley and Zachos, 2000)					2001) and confirmed using equation of (Hays and Grossman, 1991)
57	India, Lameta Formation (Maastrichtian, not uppermost Maastrichtian)	Crocodile $\delta^{18}0$	**18**	+2.1/-3°	Calculated from 95% C.I. shown in paper	16	76	-25	58	Calculated from data in (Amiot et al., 2004)
58a	Chile, Las Tablas (upper Campanian to lower Maastrichtian)	Fish tooth enamel $\delta^{18}0$	**21**	±1.2°	1 S.E. for modern calibration data, equation 2 of (Lécuyer et al., 2013)	-28	-71	-30	-57	(Puceat et al., 2007), (Lécuyer et al., 2013) recalibration
58b	Chile, Las Tablas (upper Campanian to lower Maastrichtian)	Fish tooth enamel $\delta^{18}0$	**25**	±2.7°	1 S.E. for modern calibration data, equation 2 of (Pucéat et al., 2010)	-28	-71	-30	-57	(Puceat et al., 2007), (Pucéat et al., 2010) recalibration
59a	Chile, Algarrobo (upper Campanian to lower Maastrichtian)	Fish tooth enamel $\delta^{18}0$	**20**	±1.2°	1 S.E. for modern calibration data, equation 2 of (Lécuyer et al., 2013)	-33.4	-71.7	-35	-58	(Puceat et al., 2007), (Lécuyer et al., 2013) recalibration
59b	Chile, Algarrobo (upper Campanian to lower Maastrichtian)	Fish tooth enamel $\delta^{18}0$	**24**	±2.7°	1 S.E. for modern calibration data, equation 2 of (Pucéat et al., 2010)	-33.4	-71.7	-35	-58	(Puceat et al., 2007), (Pucéat et al., 2010) recalibration
60	Madagascar (lower Maastrichtian)	Crocodile $\delta^{18}0$	**27**	+1/-2.1°	Calculated from 95% C.I. shown in paper	-20	45	-33	36	Calculated from data in (Amiot et al., 2004)

61	Madagascar (lower Maastrichtian)	Dinosaur $\delta^{18}0$	**28**	+2.3/-0.8°	Calculated from 95% C.I. shown in paper	-20	45	-33	36	Calculated from data in (Amiot et al., 2004)
62a	New Zealand (upper Campanian to Maastrichtian)	Macroflora, CLAMP	**12–14**	±2.8°	2 S.D., maximum error for CLAMP extant data set	-46	170	-58	-165	(Kennedy et al., 2002)
62b	New Zealand (upper Campanian to Maastrichtian)	Macroflora, Leaf margin analysis	**15**	±2.0°	1 S.D. sampling error for fossils	-46	170	-58	-165	(Kennedy et al., 2002)
63	Vega Island, Antarctic Peninsula (Maastrichtian)	Mollusc $\delta^{18}0$, aragonite or calcite	**9–15 (12)** n=27	±1.6°	1 S.E. of modern calibration data for mollusks in (Grossman and Ku, 1986)	-64	-57.7	-63	-67	(Pirrie and Marshall, 1990)
64	King George Island, James Ross Basin (upper Maastrichtian)	Coexistence Intervals, Flora	**14–18**	NA	MAT interval allowed by nearest living relatives	-64	-57.7	-63	-67	(Poole et al., 2005)
65	King George Island, James Ross Basin (upper Maastrichtian)	Wood anatomy	**11**	±5.4°	Maximum error for estimating MAT in modern wood assemblages with <25 species (Wiemann et al., 1998)	-64	-57.7	-63	-67	(Poole et al., 2005)
66	Seymour Island, Antarctic Peninsula (uppermost Maastrichtian)	GDGT, MBT/CBT	**10–14 (12)** n= 8	±5°	RMS error for modern MBT/CBT	-64.2	-56.6	-63	-67	(Kemp et al., 2014)

[1]The paleolatitude for Baja California is generated by the latest plate model of Christopher Scotese and represents the most northerly possible latitude for Baja California during the Maastrichtian. The authors of the original publication argue for the northward displacement of Baja California between the Maastrichtian and Recent (Maestas et al., 2003). Thus, the temperature provided in this table may represent a maximum possible $\delta^{18}0$ marine temperature for our reconstructed latitude.

Sources of data—We use a diverse set of terrestrial and marine temperature proxies to reconstruct Mean Annual Temperature (MAT). Terrestrial proxies include paleobotany, membrane lipids of soil Crenarchaeota (MBT/CBT), and $\delta^{18}O$ of tooth enamel from dinosaurs and crocodilians. Marine proxies include membrane lipids of marine Crenarchaeota (TEX_{86}) and the $\delta^{18}O$ of diverse fossils, including fish tooth enamel (phosphate), mollusk shells and fish otoliths (aragonite), and exceptionally preserved calcite ("glassy" planktonic foraminifera and well-preserved rudists and other mollusks). We restrict our analysis of $\delta^{18}O$ to remains that show little or no evidence for post-mortem alteration, to avoid the problem of diagenetic overprinting of surface water carbonate by colder bottom waters (Pearson et al., 2001). We restrict our analysis to Maastrichtian remains except in situations where it was necessary to use late Campanian remains to obtain a good latitudinal gradient (e.g. terrestrial $\delta^{18}O$).

Details are provided below.

Paleobotany—Most paleobotanical temperatures are based on the physiognomy of leaf macrofossils. We use two widely employed calibrations between leaf physiognomy and climate: 1) Leaf Margin Analysis (LMA), and 2) Climate Leaf Analysis Multivariate Program (CLAMP).

LMA uses the percentage of entire-margined (non-toothed) species of dicot leaves to estimate MAT, based on a linear calibration between MAT and the percentage of Entire-Margined Species (EMS). For Northern Hemisphere fossil assemblages, we use the calibration of Wilf for modern Northern Hemisphere floras (Wilf, 1997). We use it because: 1) it has a similar slope to other Northern Hemisphere calibrations, 2) it predicts higher tropical temperatures than other calibrations, and 3) our preliminary analysis of Western Interior assemblages using CLAMP indicates that the most similar extant assemblages are from the Northern Hemisphere. We do not use the global calibration of Peppe et al. (Peppe et al., 2011) because of its high error, which results from inclusion of assemblages from Australia and New Zealand. The leaf margin equation for extant Australian floras shows a significantly different Y intercept from that for extant Northern Hemisphere floras (Greenwood et al., 2004), and leaf margin does not predict temperature in extant New Zealand floras because nearly all woody species are evergreen (Kennedy et al., 2014).

CLAMP is a multivariate calibration that uses leaf size categories and multiple features of leaf shape, including multiple characters of the leaf margin. It uses multivariate ordination to estimate MAT, either through projection of the fossil assemblage on to the MAT axis, or through averaging temperatures of the nearest extant assemblages in multidimensional ordination space. Currently there is animated discussion in the literature about the pros and cons of CLAMP and LMA.

Both LMA and CLAMP predict similar MAT for high latitudes and the Gulf Coast of the United States. They diverge in North American assemblages ranging from 40–55° paleolatitude, with CLAMP estimating MAT up to 7°C lower than LMA. The two values have overlapping Standard Deviations (S.D.) for most floras, indicating that the estimates are probably not significantly different statistically. The reason for the bias in the two methods is not yet clear. Most CLAMP estimates of MAT for the Maastrichtian are based on early calibrations, which used a much smaller number of extant leaf assemblages than the current version of CLAMP.

Additional paleobotanical estimates of MAT come from Digital Leaf Physiognomy, Dicot Wood Physiognomy, and Coexistence Interval Analysis. Digital Leaf Physiognomy numerically analyses leaf shape to estimate MAT. It increases precision and minimizes user error by quantifying leaf traits that show continuous variation. It is also time consuming; so far, only one Maastrichtian leaf flora has used this method to estimate MAT. Wood physiognomy uses characters of dicot wood anatomy, calibrated by multiple regression, to estimate MAT. Only one Maastrichtian assemblage has used this method so far, in part because of the low number of latest Cretaceous wood floras and the time needed to make thin sections of fossil wood. Coexistence Interval Analysis uses the nearest living relatives of fossil taxa to infer climate from their area of climatic overlap. So far it has been used only for assemblages from the high southern latitudes (mostly palynomorphs), where relationships with extant genera are relatively clear.

<u>GDGT proxies</u>—The TEX_{86} proxy estimates MAT from the ratio of different glycerol dialkyl glycerol tetraethers (GDGTs) with 86 carbons, which comprise membrane lipids in marine Crenarchaeota (organisms with cell organization similar to that of bacteria but belonging to Domain Archaea, rather than Domain Eubacteria) (Schouten et al., 2002). The TEX_{86} index strongly correlates with mean surface water temperature, based predominantly on core top data. We use the TEX_{86}^{H} calibration of Kim et al. (Kim et al., 2010), based on the log of $TEX_{86,}$ because it shows the lowest core top error of all calibrations for MAT >5°C (1 S.D. = ±2.5°C). It also appears to accurately predict MAT >30° on the basis of limited mesocosm data. We converted all published TEX_{86} values into TEX_{86}^{H} temperatures.

TEX_{86}^{H} tends to give higher temperature estimates than other geochemical and paleobotanical proxies. The 1 S.D. error bars of TEX_{86}^{H} and the other proxies overlap at lower latitude sites, but do not overlap at high latitude sites. One of the two warm outliers for the Arctic is the TEX_{86}^{H} data point of Jenkyns et al. (Jenkyns et al., 2004), which is at least 2 S.D. higher than any other Arctic temperature estimate. Spicer and Herman (Spicer and Herman, 2010) make the argument that, in polar environments, the TEX_{86} proxy shows a strong summer bias.

The MBT–CBT proxy is based on the distribution of branched glycerol dialkyl glycerol tetraether (brGDGT) membrane lipids, which comprise membrane lipids of soil Crenarchaeota. The one MBT-CBT data point (Antarctic Peninsula) gives MAT estimates comparable to those of other proxies.

Marine stable isotopes—An important part of our data base for lower and middle latitudes is the $\delta^{18}O$ of carbonate and phosphate. For carbonate, we were extremely selective and only used fossils that showed evidence for minimal or no diagenesis. For calcite, we only used : 1) "glassy" planktonic foraminifera, 2) other planktonic foraminifera that showed well-preserved microstructure under SEM and the absence of secondary calcite, and 3) exceptionally preserved calcite in rudist bivalves. For aragonite, which is thermodynamically less stable than calcite, we used published data for mollusks, provided there was no evidence for diagenesis or significant freshwater influence. For calcite, we used the calibration of Hays and Grossman (Hays and Grossman, 1991). For aragonite, we used the calibration of Grossman and Ku (Grossman and Ku, 1986).

The phosphate of fish tooth enamel is thought to be less vulnerable to diagenetic alteration than calcite. We recalculated all published values for fish tooth enamel because the calibrations have changed since the last comprehensive analysis of Cretaceous fish tooth enamel (Puceat et al., 2007). We use two calibrations: 1) equation 2 in Puceat et al. (Pucéat et al., 2010), and 2) equation 2 in Lecuyer et al. (Lécuyer et al., 2013).

The Puceat et al. equation is based on $\delta^{18}O$ of phosphate from fish tooth enamel in both natural and mesocosm environments, whereas the Lecuyer et al. equation is based on $\delta^{18}O$ of phosphate in lingulid brachiopods and the teeth of a small number of fish. Both calibrations have a similar slope to the older calibration, but give temperatures at least 4°C higher. Temperatures based on the Puceat et al. calibration are, on average, 3°C higher than those based on the Lecuyer et al. calibration. When recalculating temperatures with the Puceat et al. calibration, we added 2.2‰ to $\delta^{18}O$ values from early studies that use older analytical methods and calibrations, and added 0.9‰ to $\delta^{18}O$ values from later studies that use current analytic methods, in particular precipitating silver phosphate (Pucéat et al., 2010). Both corrections include recalibration of the standard NBS120c. When recalculating temperatures from older data using the Lecuyer et al. calibration, we subtracted 0.9‰ from the 2.2‰ correction because this calibration uses an older value for NBS120c.

In our recalculations, we follow other authors and assume that latest Cretaceous seawater had a $\delta^{18}O$ of -1‰ SMOW, namely, seawater in an ice-free world. Isotopic temperatures were calculated from values of $\delta^{18}O$ adjusted for latitude, using the formula derived for modern oceans by Bice et al. (2000) and SMOW = -1‰. These were checked for consistency with values of $\delta^{18}O$ derived from the model's sea surface salinity fields, using the formula of Broecker (1989). When the salinity-derived values differed >0.8‰ from the latitudinally adjusted values and at least one of the values was -1‰ or below (Tanzania, Oman, Texas, and most sites at middle to high latitudes), we used the average SMOW value of -1‰ to calculate temperatures. We used "best estimates" of $\delta^{18}O$ because the low-resolution version of CCSM3 does not simulate stable isotopes.

Terrestrial stable isotopes—We include data from terrestrial stable isotopes for the sake of completeness, but are well aware of the potential problems surrounding the use of $\delta^{18}O$ in meteoric water to estimate past surface temperatures (Fricke and O'Neil, 1999; Kohn and Welker, 2005; Suarez et al., 2013; Ufnar et al., 2002). Most temperatures are calculated from the $\delta^{18}O$ values provided by Amiot et al. (Amiot et al., 2004) for

dinosaur and crocodile tooth enamel, which were obtained by subtracting 21.9‰ from the $\delta^{18}O$ values listed for bone, and using the resulting value in their equation 3.

MAT calculated from the $\delta^{18}O$ of vertebrate tooth enamel and pedogenic carbonate tends to be lower than that based on other proxies. For Texas and India, the values are so low as to constitute outliers. However, the latitudinal gradient of MAT based on terrestrial isotopic data is similar to that of some other proxies, and the best model simulations.

Calculation of error—We calculated errors for our paleotemperatures to determine which proxies give significantly different temperatures, and to evaluate the goodness of fit between proxies and model simulations (see below). The two major types of error used here are: 1) error introduced by the choice of calibration, and 2) random error found in the calibration data set or fossil assemblage.

Choice of calibration—As discussed above, we used two major calibrations for leaf physiognomy and fish tooth enamel because of the absence of consensus regarding the most accurate method. In other cases, we used the calibration chosen by the authors of the original publication, or a commonly used calibration from the literature that is capable of estimating temperatures over a wide range.

Sampling error with modern calibrations or fossil assemblages—The second type of error varied between proxy and calibration, and was handled in different ways for different proxies and calibration. All reported errors are either 1 Standard Deviation (S.D.) or 1 Standard Error (S.E.), depending on how error was calculated in the original publication. We used 1 S.E. when calculating our own sampling error for modern calibrations.

Different types of error are used for: 1) MBT/CBT, which is Root Mean Squared (RMS) error, 2) dicot wood physiognomy, which is the maximum error in estimating MAT from a low diversity assemblage, and 3) terrestrial $\delta^{18}O$, which uses the 95% Confidence Interval around the mean $\delta^{18}O$ value reported in the publication.

For plotting model data fits, we used the mean value for the proxy record, 1 S.D./S.E. above the highest measured value, and 1 S.D./S.E. below the lowest measured value, to calculate the range of error. No error is calculated for interval data, because the true value could lie anywhere with the interval. Here, the midpoint substituted for the mean, and the high and low values of the range substituted for error.

Paleobotany—For LMA, we estimate error as 1 S.E. of the calibration data set (±2°C) or 1 S.D. of the sampling error for the fossil assemblage, whichever is greater (Wilf, 1997). For CLAMP, we use the largest error in the calibration data cited on the CLAMP website (1 S.D. = ±2.8°C). For Digital Leaf Physiognomy, we used the error figure cited by the authors for the Northern Hemisphere calibration (Peppe et al., 2011) (1 S.E. =

±3.3°C). Interval analysis does not calculate means, and therefore has no error in the sense of other estimates. The interval represents the possible range of climates under which the flora could have existed, and the actual value can lie anywhere within the interval.

TEX_{86}—As mentioned earlier, we chose the TEX_{86}^{H} calibration (Kim et al., 2010) because of its low standard deviation relative to other calibrations (1 S.D. = ±2.5°C, core top error).

Marine $\delta^{18}O$—Although regression equations are used to estimate paleotemperature from $\delta^{18}O$, the original publications tend not to provide any estimate of calibration error. For calcite from planktonic foraminifera, Holocene core top data estimate error of 1 S.D. = ±2.9°C (Crowley and Zachos, 2000). For aragonite, our regression of the calibration data (Grossman and Ku, 1986) estimates error of 1 S.E. = ±1.6°C (mollusk data only). Fish otoliths are reported to have comparable calibration error to macroinvertebrate aragonite (Thorrold et al., 1997). For fish tooth enamel, our regression of the calibration data estimates error of 1 S.E. = ±2.7°C for the Puceat et al. calibration, and 1 S.E. = ±1.2°C for the Lecuyer et al. calibration (Lécuyer et al., 2013; Pucéat et al., 2010).

Terrestrial $\delta^{18}O$—As mentioned previously, error provided for $\delta^{18}O$ of apatite represents the 95% Confidence Interval around the mean $\delta^{18}O$ for each site (dinosaur and crocodilian values calculated separately)(Amiot et al., 2004). Equation 2, which describes the relation between vertebrate phosphate $\delta^{18}O$ and latitude, has significant error that might easily exceed the error of $\delta^{18}O$ measured for fossils (maximum spread of values ≈ ±9‰, which gives a maximum spread of estimated MAT ≈ ±18°C). However, we did not have access to the actual measurements that were used to derive the equation, so we did not calculate calibration error.

PART 2: REANALYSIS OF LEAF MACROFLORAS FOR NORTH AMERICA

We recalculated temperatures for the North American Maastrichtian macrofloras reported by Wolfe and Upchurch (Wolfe and Upchurch, 1987) using leaf margin analysis; these values are reported in Supplementary Data, Part I. We recalculated leaf margin temperatures for two reasons. First, Jack Wolfe did the analysis of Maastrichtian assemblages, while Garland Upchurch did all of the Albian and most of the Cenomanian assemblages. We wished to re-evaluate species delimitations, which can have a major effect on calculated temperature. Second, we used the calibration equation of Wilf (Wilf, 1997) because the calibration used by Wolfe and Upchurch is inaccurate (Greenwood et al., 2004). Leaf margin analyses of North American Cretaceous floras published over the past decade use either the Wilf equation or another similar equation, based on extant floras of North America and East Asia. The Wilf equation also gives the highest MAT of any leaf margin equation, especially for assemblages with high percentages of entire-margined species.

We added two unpublished assemblages not available to Wolfe and Upchurch: 1) an assemblage from the Jose Creek member of the McRae Formation, which is preserved in recrystallized volcanic ash, and 2) the Broomfield assemblage of the Laramie Formation, which is preserved in sandstone. Jacqueline Scherer and Garland Upchurch analyzed the Jose Creek flora, while Garland Upchurch analyzed the Broomfield assemblage. The Broomfield assemblage is based on Upchurch's unpublished report to the Colorado Department of Transportation. We also recalculated mean annual temperature for the Littleton assemblage from the Denver Basin, which was never monographed but reported in Wolfe and Upchurch.

We calculated a maximum possible mean annual temperature for the Sable Mountain flora of the Cantwell Formation (Tomisch et al., 2010), coding all the species with missing margins as entire-margined. We did this to determine whether leaf margin data could produce a mean annual temperature as warm as CLAMP.

Our reanalysis gives a percentage of entire-margined species for each flora that usually is within five percent of the values published by Wolfe and Upchurch (±1.4°C). The exception is the Laramie flora, which has a percentage of entire-margined species twelve percent higher (+3.4°C).

The floras, their percentage of entire-margin species, and calculated mean annual temperatures are below. The floras are arranged from low to high paleolatitude. When a species varied between entire and non-entire margined, it was coded as 0.5 entire margined.

Flora	Number of dicot species	Number Entire-Margined Species	Number of species, margins entire to non-entire	Percent Entire-Margined Species	Mean Annual Temperature, °C
Cooper assemblage, McNairy Formation	36	25	0	69	**22**
Perry assemblage, McNairy Formation	46	32	1	71	**23**
Jose Creek Member, McRae Formation	42	27	1	68	**22**
Vermejo Formation	64	47	0	73	**23**
Raton Formation (Maastrichtian part only)	43	31	0	72	**23**
Laramie Formation (based on illustrated species in Knowlton's monograph)	69	57	0	83	**26**
Laramie Formation, Broomfield locality	20	14	1	73	**23**
Denver Formation, Littleton assemblage	50	35	1	71	**23**
Medicine Bow Formation	39	24	0	62	**20**
Lance Formation	39	24	1	63	**20**
Cantwell Formation, Sable Mountain assemblage	23	≤5	0	≤22	**≤8**

The temperature equation of Wilf is as follows:

MAT (°C) = 2.24 + (0.286 x %Entire-margined species).

PART 3: THE VILYUI BASIN MACROFLORA

Spicer and coworkers (Spicer et al., 2008) provide macrofloral and palynofloral evidence on the temperature of the Late Cretaceous Vilyui Basin flora. The macroflora is Cenomanian in age (Spicer and Herman, 2010), while the palynoflora is younger (Spicer, written communication, August 2010). Spicer and coworkers ran climate model simulations using Cenomanian, Turonian, and Maastrichtian geographies but could not match the mean annual temperature, warm month mean, or cold month mean provided by the macroflora.

We adjusted the mean annual temperature (MAT) of the Cenomanian macroflora to compare with our Maastrichtian model runs. We did this in two steps. First, we took the graph of the CLAMP latitudinal gradient from figure 9 in Spicer and Herman (Spicer and Herman, 2010) and moved the Vilyui macroflora temperature from the Cenomanian gradient line to the Maastrichtian gradient line at the same paleolatitude. This changed MAT by -3.5°C. Next, we moved the Vilyui Basin 4 degrees south along the Maastrichtian gradient line to accommodate plate motion between the Cenomanian and Maastrichtian, using plate positions for ~95 mya and 65 mya (Figure 1). This increased MAT by 0.8°C (+4° latitude x 0.2°C per degree latitude). The net change in MAT is -2.7°C.

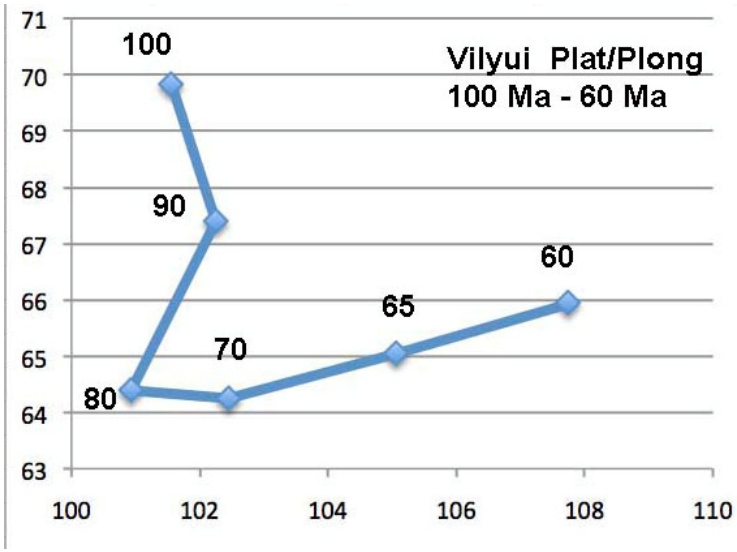

Figure DR1. Late Cretaceous movement of the Vilyui Basin, based on the current version of Point Tracker software.

The adjusted MAT is 11.3°C. Our warmest simulations produce comparable or warmer temperatures, but with significantly greater seasonality than allowed by data.

The seasonality issue for the Vilyui Basin may be a function of reconstructed paleogeography (Figure 2). Markwick and Valdes (Markwick and Valdes, 2004), who provided the paleogeography for Spicer et al. (Spicer et al., 2008), reconstruct Late Cretaceous paleogeography for Siberia similar to that of Upchurch et al. (Upchurch et al., 1999), with mountains present to the east and south, and fully continental conditions for the Vilyui Basin. However, the paleogeography of Kasmin et al. (Kazmin et al., 1998) reconstructs the Vilyui Basin with a narrow seaway during the Late Cretaceous (Figure 2), which becomes a complex of lakes and marshes by the Maastrichtian, and fully terrestrial during the Paleocene.

The degree of seasonality for the Vilyui Basin in model simulations probably shows a strong relation to the presence/absence of large lake or narrow seaway, and whether or not a particular climate model has sufficiently high spatial resolution to incorporate this feature of paleogeography. However, no model simulations have yet tested this idea.

Figure DR2. Latest Cretaceous paleogeography of the Vilyui Basin, showing the presence of a large lake (Kazmin et al., 1998).

PART 4: MODEL-DATA COMPARISONS

This section provides additional plots of model output and proxy data.

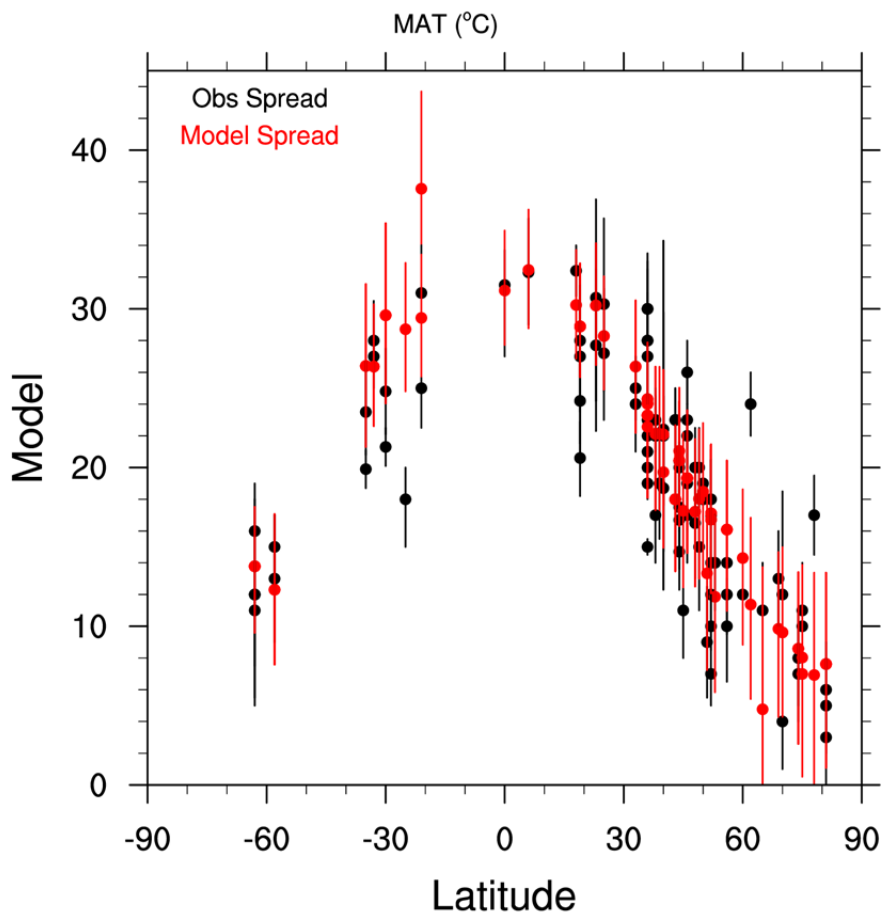

Figure DR3. Plot showing range of temperature values for model simulations (red) and proxies (black). The dots represent sites with proxy data. The black dots represent mean values for the proxy, and the black lines represent error as described in Part 1. The red dots represent the median value from all model simulations, and the red lines represent the maximum and minimum values.

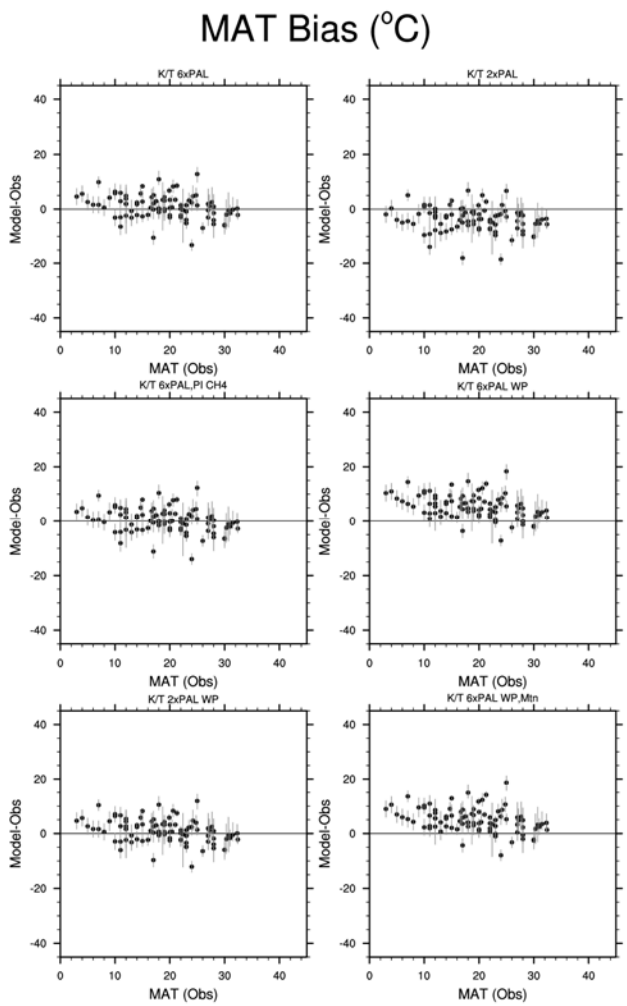

Figure DR4. Plot of model-observed vs. observed Mean Annual Temperature (MAT). Note how the three simulations on the left show no strong bias and a fairly even spread around the 0 line. In contrast, the 2xPAL simulation is too cold, and the 6xPAL WP simulations are too hot.

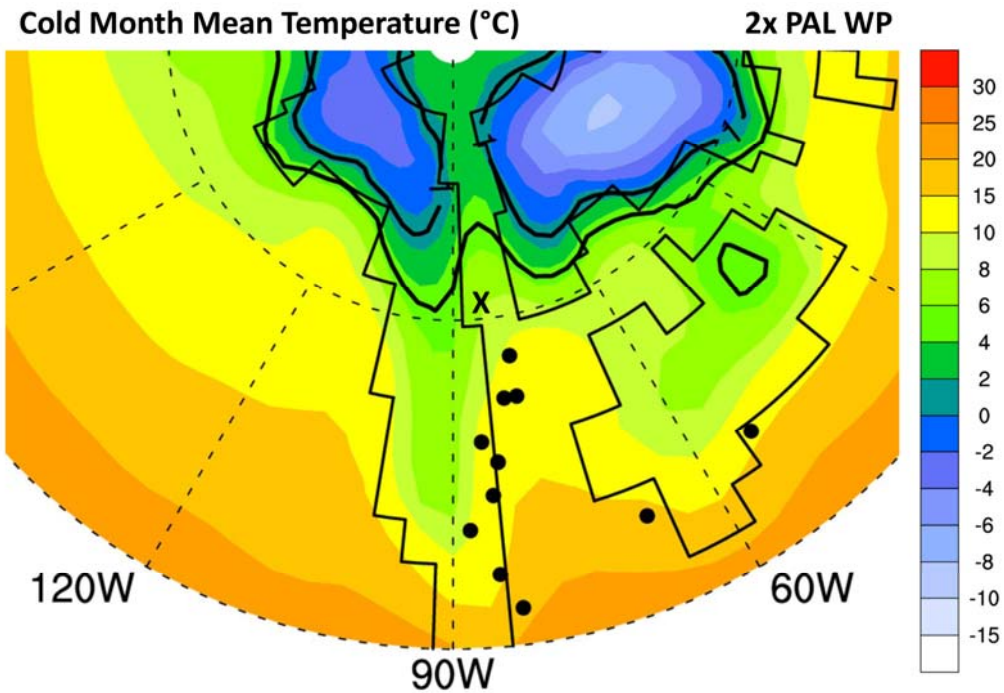

Figure DR5. Simulated Cold Month Mean Temperature (CMMT) for North America and surrounding regions, 2x PAL WarmPole simulation, and the distribution of crocodilians and palm macrofossils (points) that come from localities listed in Part 1. The two solid black lines represent the 1°C and 5°C CMMT isotherm simulated by the model. The dashed circular lines represent 30°N and 60°N paleolatitude. Extant crocodilians and palms are restricted to climates with CMMT >5°C. **X** denotes our northernmost data point shifted to its latitudinal position in Markwick (Markwick, 2007). Note how all our data points lie within the zone of Crocodile and Palm climate. In contrast, the simulations of Markwick (Markwick, 2007) and Upchurch et al. (Upchurch et al., 1999) are too cold to simulate the full distribution of crocodilians and palm macrofossils.

Figure DR6. 2xCO_2 WarmPole simulation, marine data points with temperature values for regions where the model simulates tropical temperatures (Mean Annual Surface Temperature ≥25°C). Black circles with labels = regions where the average proxy temperature and model temperature agree. Purple stars = regions where the average proxy temperature exceeds the model temperature. Blue stars = regions where the average proxy temperature is less than the model temperature. Note how the number of purple stars is slightly higher than the number of blue stars, indicating that the model does not consistently overestimate tropical temperatures. The high range of temperatures for Israel reflects major differences between temperatures calculated from fish tooth enamel (mean = 21 or 24°C) and TEX_{86} (mean = 27 or 28°C).

Average model temperatures for the 6xCO_2 simulations and the 2xCO_2 Warmpole simulation are slightly higher than the proxy temperatures when both calibrations for fish tooth enamel are used. In contrast, average model temperatures for these simulations are **slightly lower** than proxy temperatures when only the warmer calibration for fish tooth enamel is used. This indicates that modeled tropical marine temperatures are high, but do not exceed the uppermost limit allowed by proxies. See table 1 for details.

TABLE DR1. MEAN ANNUAL SURFACE TEMPERATURE (MAT), MODEL SIMULATIONS

Simulation	CO_2 ppm	CH_4 ppb	Liquid clouds	Global MAT	Tropical (20°S–20°N) MAT	Vilyui Basin MAT	MAT gradient, 30°N –80°N, grid points with geologic data	MAT gradient, 30°N –80°N, zonal average
2xCO_2	560	2000	Standard	19.6°	28.3°	-2.8°	0.46°	0.44°
6xCO_2	1680	2000	Standard	23.8°	31.9°	4.6°	0.40°	0.37°
6xCO_2, PIL methane	1680	760	Standard	23.2°	31.4°	2.9°	0.42°	0.37°
2xCO_2 WP	560	2000	Warmpole	23.7°	31.7°	5.0°	0.40°	0.36°
6xCO_2, WP	1680	2000	Warmpole	27.9°	35.5°	11.9°	0.36°	0.32°
6xCO_2, WP flat Siberia	1680	2000	Warmpole	27.9°	35.5°	13.7°	0.38°	0.33°

Note: Surface temperatures are in °C for 2m height (TREFHT). Zonal average is for all model grid points, and includes interior and high elevation regions with no geologic data. Warmpole clouds (WP) cause average global warming similar to a tripling of atmospheric CO_2. Adjusted CLAMP temperature for the Vilyui Basin is 11.3°C. MAT gradient 30°N –80°N based on geologic data is 0.38–0.40°C.

TABLE DR2. STATISTICS FOR MODEL-DATA COMPARISIONS

Simulation	**6xCO_2**	**2xCO_2**	**6xCO_2 PAL CH_4**	**6xCO_2 WarmPole**	**2xCO_2 WarmPole**	**6xCO_2 WarmPole No Siberian Mts.**
Average Global Temperature, °C	23.8	19.6	23.2	27.9	23.7	27.9
Average (model-observed), all latitudes and data	0.51	-4.22	-0.09	5.08	0.61	4.59
Standard Deviation (model-observed), all latitudes and data	4.1	4.2	4.1	4.0	3.9	4.0
Average (model-observed), 30°N to 30°S, all data	3.21	-0.96	2.62	7.42	2.93	7.46
Standard Deviation (model-observed), 30°N to 30°S, all data	4.3	3.6	4.3	4.8	4.0	4.8
Average (model-observed), 30°N to 30°S, marine data only	2.19	-1.77	1.61	6.31	1.96	6.32
Standard Deviation (model-observed), 30°N to 30°S, marine data only	3.3	3.0	3.3	3.7	3.1	3.8
Average (model-observed), marine data only, regions with model SST ≥25°C, all data	1.54	-2.49	0.96	5.63	1.26	5.61
Standard deviation (model-observed), marine data only, regions with model SST ≥25°C, all data	3.8	3.4	3.8	4.3	3.6	4.4
Average (model-observed), marine data only, regions with model SST ≥25°C, without Lecuyer data	-0.01	-3.86	-0.58	3.94	-0.23	3.92
Standard Deviation (model-observed), marine data only, model SST $\geq 25°C$, without Lecuyer data	2.8	2.5	2.8	2.6	2.6	3.3

REFERENCES CITED

Alsenz, H., J, R., Ashckenazi-Polivoda, S., Meilijson, A., Ron-Yankovich, L., Abramovich, S., Illner, P., Almogi-Labin, A., Feinstein, S., Berner, Z., and Püttmann, W., 2013, Sea surface temperature record of a Late Cretaceous tropical Southern Tethys upwelling system: Palaeogeography, Palaeoclimatology, Palaeoecology, v. 392, p. 350-358.

Amiot, R., Lecuyer, C., Buffetaut, E., Fluteau, F., Legendre, S., and Martineau, F., 2004, Latitudinal temperature gradient during the Cretaceous Upper Campanian-Middle Maastrichtian: $d^{18}O$ record of continental vertebrates: Earth and Planetary Science Letters, v. 226, p. 255-272.

Ashckenazi-Polivoda, S., Rak, C., Almogi-Labin, A., Zsolt, B., Ovadia, O., and Abramovich, S., 2014, Paleoecology of the K-Pg mass extinction survivor Guembelitria (Cushman): isotopic evidence from pristine foraminifera from Brazos River, Texas (Maastrichtian): Paleobiology, v. 40, p. 24-33.

Carpenter, S.J., Erickson, J.M., and Holland Jr., F.D., 2003, Migration of a Late Cretaceous fish: Nature, v. 423, p. 70-74.

Crowley, T.J., and Zachos, J.C., 2000, Comparison of zonal temperature profiles for past warm periods, *in* Huber, B.T., MacLeod, K.G., and Wing, S.L., eds., Warm Climates in Earth History: Cambridge, Cambridge University Press, p. 50-76.

Dworkin, S., Nordt, L., and Atchley, S., 2005, Determining terrestrial paleotemperatures using the oxygen isotopic composition of pedogenic carbonate: Earth and Planetary Science Letters, v. 237, p. 56-68.

Estrada-Ruiz, E., Upchurch, G.R., and Cevallos-Ferriz, S.R.S., 2008, Flora and climate of the Olmos Formation (Upper Campanian-Lower Maastrichtian), Coahuila, Mexico: a preliminary report: Gulf Coast Association of Geological Societies Transactions, v. 58, p. 273-283.

Fricke, H.C., and O'Neil, J.R., 1999, The correlation between 18O=16O ratios of meteoric water and surface temperature: its use in investigating terrestrial climate change over geologic time: Earth and Planetary Science Letters, v. 170, p. 181-196.

Goloneva, L.B., 2000, The Maastrichtian (Late Cretaceous) climate in the Northern Hemisphere, *in* Hart, M.B., ed., Climates: Past and Present, Volume 181: Geological Society Special Publication: London, The Geological Society, p. 43-54.

Greenwood, D.R., Wilf, P., Wing, S.L., and Christophel, D.C., 2004, Paleotemperature estimation using leaf-margin analysis: is Australia different?: Palaios, v. 19, p. 129-142.

Grossman, E.L., and Ku, T.L., 1986, Oxygen and carbon isotope fractionation in biogenic aragonite: temperature effects: Chemical Geology (Isotope Geoscience Section), v. 59, p. 59-74.

Hays, P.D., and Grossman, E.L., 1991, Oxygen isotopes in meteoric calcite cements as indicators of continental paleoclimate: Geology, v. 19, p. 441-444.

Jenkyns, H.C., Forster, A., Schouten, S., and Damste, J.S.S., 2004, High temperatures in the Late Cretaceous Arctic Ocean: Nature, v. 432, p. 888-892.

Kazmin, V.G., Natapov, L.M., Bush, W.A., Filipova, I.B., Jasamanov, N.A., Balukhovsky, A.N., Volkov, J.V., Gatinsky, J., Kalimulin, S.M., Kulikova, L.I., Miledin, A.K., Pugacheva, I.P., Suetenko, O.D., Bocharova, N.J., Zonenshain, L.P., Kononov, M.K., and Scotese, C.R., 1998, The Paleogeographic Atlas of Northern Eurasia: Moscow, Institute of Tectonics of Lithospheric Plates, Institute of Lithospheric Plates,, 26 maps p.

Kemp, D.B., Robinson, S.A., Crame, J.A., Francis, J.E., Ineson, J., Whittle, R.J., Bowman, V., and O'Brien, C., 2014, A cool temperate climate on the Antarctic Peninsula through the latest Cretaceous to early Paleogene: Geology, v. 42, p. 583-586.

Kennedy, E.M., Arens, N.C., Reichgelt, T., Spicer, R.A., Spicer, T.E.V., Stranks, L., and Yang, J., 2014, Deriving temperature estimates from Southern Hemisphere leaves: Palaeogeography, Palaeoclimatology, Palaeoecology, v. 412, p. 80-90.

Kennedy, E.M., Spicer, R.A., and Rees, P.M., 2002, Quantitative palaeoclimate estimates from Late Cretaceous and Paleocene leaf floras in the northwest of the South Island, New Zealand: Palaeogeography, Palaeoclimatology, Palaeoecology, v. 184, p. 321-345.

Kim, J.-H., Meer, J.v.d., Schouten, S., Helmke, P., Willmott, V., Sangiorgi, F., Koc, N.n., Hopmans, E.C., and Damste´, J.S.S., 2010, New indices and calibrations derived from the distribution of crenarchaeal isoprenoid tetraether lipids: Implications for past sea surface temperature reconstructions: Geochimica et Cosmochimica Acta, v. 74, p. 4639-4654.

Kohn, M.J., and Welker, J.M., 2005, On the temperature correlation of ^{18}O in modern precipitation: Earth and Planetary Science Letters, v. 231, p. 87-96.

Lécuyer, C., Amiot, R., Touzeau, A., and Trotter, J., 2013, Calibration of the phosphate δ18O thermometer with carbonate–water oxygen isotope fractionation equations: Chemical Geology, v. 347, p. 217-226.

Linnert, C., Robinson, S.A., Lees, J.A., Bown, P.R., Perez-Rodrıguez, I., Petrizzo, M.R., Falzoni, F., Littler, K., Arz, J.A., and Russell, E.E., 2014, Evidence for global cooling in the Late Cretaceous: Nature Communications, v. DOI: 10.1038/ncomms5194.

Maestas, Y., MacLeod, K.G., Douglas, R., Self-Trail, J., and Ward, P.D., 2003, Late Cretaceous foraminifera, paleoenvironments, and paleoceanography of the Rosario Formation, San Antonio Del Mar, Baja Califorina, Mexico: Journal of Foraminiferal Research, v. 33, p. 179-191.

Markwick, P.J., 1998, Fossil crocodilians as indicators of Late Cretaceous and Cenozoic climates: implications for using palaeontological data in reconstructing palaeoclimate: Palaeogeography, Palaeoclimatology, Palaeoecology, v. 137, p. 205-271.

Markwick, P.J., 2007, The palaeogeographic and palaeoclimatic significance of climate proxies for data-model comparisons, *in* Williams, M., Haywood, A.M., Gregory, F.J., and Schmidt, D.N., eds., Deep-Time Perspectives on Climate Change. Marrying the Signal from Computer Models and Biological Proxies: London, The Geological Society, p. 251-312.

Markwick, P.J., and Valdes, P.J., 2004, Palaeo-digital elevation models for use as boundary conditions in coupled ocean-atmosphere GCM experiments: a Maastrichtian (late Cretaceous) example: Palaeogeography, Palaeoclimatology, Palaeoecology, v. 213, p. 37-63.

Moiseeva, M.G., 2005, Members of the angiosperm genus *Cissites* from the Maastrichtian Koryak flora, northeastern Russia.: Paleontological Journal, v. 39, p. 548-556.

Ounis, A., Kocsis, L., Chaabani, F., and Pfeifer, H.-R., 2008, Rare earth elements and stable isotope geochemistry ($\delta^{13}C$ and $\delta^{18}O$) of phosphorite deposits in the Gafsa Basin, Tunisia: Palaeogeography, Palaeoclimatology, Palaeoecology, v. 268, p. 1-18.

Parrish, J.T., and Spicer, R.A., 1988, Late Cretaceous terrestrial vegetation: a near-polar temperature curve: Geology, v. 16, p. 22-25.

Pearson, P.N., Ditchfield, P.W., Singano, J.M., Harcourt-Brown, K.G., Nicholas, C.J., Olsson, R.K., Shackleton, N.J., and Hall, M.A., 2001, Warm tropical sea surface temperatures in the Late Cretaceous and Eocene epochs: Nature, v. 413, p. 481-487.

Peppe, D.J., Royer, D.L., Cariglino, B., Oliver, S.Y., Newman, S., Leight, E., Enikolopov, G., Fernadez-Burgos, M., Herrera, F., Adams, J.M., Correa, E., Currano, E.D., Erickson, J.M., Hinojosa, L.F., Hoganson, J.W., Iglesias, A., Jaramillo, C., Johnson, K.R., Jordan, G.J., Kraft, N.J.B.,

Lovelock, E.C., Lusk, C.H., Niinemets, U., Penuelas, J., Rapson, G., Wing, S.L., and Wright, I.J., 2011, Sensitivity of leaf size and shape to climate: global patterns and paleoclimatic implications: New Phytologist, v. 190, p. 724-739.

Pirrie, D., and Marshall, J.D., 1990, High-latitude Late Cretaceous paleotemperatures: New data from James Ross Island, Antarctica: Geology, v. 18, p. 31-34.

Poole, I., Cantrill, D., and Utescher, T., 2005, A multi-proxy approach to determine Antarctic terrestrial palaeoclimate during the Late Cretaceous and Early Tertiary: Palaeogeography, Palaeoclimatology, Palaeoecology, v. 222, p. 95-121.

Pucéat, E., Joachimski, M.M., Bouilloux, A., Monna, F., Bonin, A., Motreuil, S., Morinière, P., Hénard, S., Mourin, J., Dera, G., and Quesne, D., 2010, Revised phosphate–water fractionation equation reassessing paleotemperatures derived from biogenic apatite: Earth and Planetary Science Letters, v. 298, p. 135-142.

Puceat, E., Lecuyer, C., Donnadieu, Y., Naveau, P., Cappetta, H., Ramstein, G., Huber, B.T., and Kriwet, J., 2007, Fish tooth d^{18}O revising Late Cretaceous meridional upper ocean water temperature gradients: Geology, v. 35, p. 107-110.

Schouten, S., Hopmans, E.C., Scheffuss, E., and Damste, J.S.S., 2002, Distributional variations in marine crenarchaeotal membrane lipids: a new tool for reconstructing ancient sea water temperatures?: Earth and Planetary Science Letters, v. 204, p. 265-274.

Spicer, R.A., Ahlberg, A., Herman, A.B., Hofmann, C.C., Raikevich, M., Valdes, P.J., and Markwick, P.J., 2008, The Late Cretaceous continental interior of Siberia: A challenge for climate models: Earth and Planetary Science Letters, v. 267, p. 228-235.

Spicer, R.A., and Herman, A.B., 2010, The Late Cretaceous environment of the Arctic: A quantitative reassessment based on plant fossils: Palaeogeography, Palaeoclimatology, Palaeoecology, v. 295, p. 423-442.

Steuber, T., Rauch, M., Masse, J.-P., Graaf, J., and Malkoc, M., 2005, Low-latitude seasonality of Cretaceous temperatures in warm and cold episodes.: Nature, v. 437, p. 1341-1344.

Suarez, C.A., Ludvigson, G.A., Gonzalez, L.A., Fiorillo, A.R., Flaig, P.P., and McCarthy, P.J., 2013, Use of multiple oxygen isotope proxies for elucidating Arctic Cretaceous palaeo-hydrology, *in* Bojar, A.V., Melinte-Dobrinescu, M.C., and Smit, J., eds., Isotopic Studies in Cretaceous Research: London, Geological Society, London.

Thorrold, S.R., Campana, S.E., Jones, C.M., and Swart, P.K., 1997, Factors determining ^{13}C and ^{18}O fractionation in aragonitic otoliths of marine fish.: Geochimica et Cosmochimica Acta, v. 61, p. 2909-2919.

Tomisch, C.S., McCarthy, P.J., Fowell, S.J., and Sunderlin, D., 2010, Paleofloristic and paleoenvironmental informatoin from a Late Cretaceous (Maastrichtian) flora of the lower Cantwell Formation near Sable Mountain, Denali National Park, Alaska: Palaeogeography, Palaeoclimatology, Palaeoecology, v. 295, p. 389-408.

Ufnar, D.F., Gonzalez, L.A., Ludvigson, G.A., Brenner, R.L., and Witzke, B.J., 2002, The mid-Cretaceous water bearer: isotope mass balance quantification of the Albian hydrologic cycle: Palaeogeography, Palaeoclimatology, Palaeoecology, v. 188, p. 51-71.

Upchurch, G.R., Otto-Bliesner, B.L., and Scotese, C.R., 1999, Terrestrial vegetation and its effects on climate during the latest Cretaceous: Geological Society of America Special Paper, v. 332, p. 407-426, 434-436.

Vellekoop, J., Sluijs, A., Smit, J., Schouten, S., Weijers, J.W.H., Damstéc, J.S.S., and Brinkhuis, H., 2014, Rapid short-term cooling following the Chicxulub impact at the Cretaceous–Paleogene boundary: Proceedings of the National Acadamy of Sciences USA, v. 111, p. 7537-7541.

Weidman, C.R., Jones, G.A., and Lohman, K.C., 1994, The long lived mollusc *Arctica islandica*: A new paleoceanographic tool for the reconstruction of bottom temperatures for the continental shelves of the northern North Atlantic Ocean: Journal of Geophysical Research, v. 99, p. 18305-18314.

Wiemann, M.C., Wheeler, E.A., Manchester, S.R., and Portier, K.M., 1998, Dicotyledonous wood anatomical characters as predictors of climate: Palaeogeography, Palaeoclimatology, Palaeoecology, v. 139, p. 83-100.

Wilf, P., 1997, When are leaves good thermometers? A new case for Leaf Margin Analysis: Paleobiology, v. 23, p. 373-390.

Wilf, P., Johnson, K.R., and Huber, B.T., 2003, Correlated terrestrial and marine evidence for global climate changes before mass extinction at the Cretaceous-Paleogene boundary: Proceedings of the National Acadamy of Sciences USA, v. 100, p. 599-604.

Wilson, P.A., and Opdyke, B.N., 1996, Equatorial sea-surface temperatures for the Maastrichtian revealed through remarkable preservation of metastable carbonate: Geology, v. 24, p. 555-558.

Wolfe, J.A., 1990, Paleobotanical evidence for a marked temperature increase following the Cretaceous/Tertiary boundary: Nature, v. 343, p. 153-156.

Wolfe, J.A., and Upchurch, G.R., 1987, North American nonmarine climates and vegetation during the Late Cretaceous: Palaeogeography, Palaeoclimatology, Palaeoecology, v. 61, p. 33-77.

Zakharov, Y.D., Popov, A.M., Shigeta, Y., Smyshlyaeva, O.P., Sokolova, E.A., Nagendra, R., Velivetskaya, T.A., and Afanasyeva, T.B., 2006, New Maastrichtian oxygen and carbon isotope record: Additional evidence for warm low latitudes: Geosciences Journal, v. 10, p. 347-367.